Journal of Solid State Chemistry 184 (2011) 698–704

Contents lists available at ScienceDirect

Journal of Solid State Chemistry

journal homepage: www.elsevier.com/locate/jssc

High-temperature crystal structure and transport properties of the layered cuprates Ln_2CuO_4, Ln=Pr, Nd and Sm

M.S. Kaluzhskikh [a], S.M. Kazakov [a], G.N. Mazo [a], S.Ya. Istomin [a,*], E.V. Antipov [a], A.A. Gippius [b], Yu. Fedotov [c], S.I. Bredikhin [c], Yi Liu [d], G. Svensson [d], Z. Shen [d]

[a] Department of Chemistry, Moscow State University, Leninskie Gory, 119991 Moscow, Russia
[b] Department of Physics, Moscow State University, Leninskie Gory, 119991 Moscow, Russia
[c] Institute of Solid State Physics RAS, 142432 Chernogolovka, Moscow Region, Russia
[d] Department of Materials and Environmental Chemistry, Stockholm University, S-10691 Stockholm, Sweden

ARTICLE INFO

Article history:
Received 7 December 2010
Received in revised form
15 January 2011
Accepted 20 January 2011
Available online 3 February 2011

Keywords:
High-temperature crystal structure
High-temperature conductivity
Cuprates
Oxygen diffusion
SIMS

ABSTRACT

High-temperature crystal structure of the layered cuprates Ln_2CuO_4, Ln=Pr, Nd and Sm with tetragonal T′-structure was refined using X-ray powder diffraction data. Substantial anisotropy of the thermal expansion behavior was observed in their crystal structures with thermal expansion coefficients (TEC) along a- and c-axis changing from TEC(a)/TEC(c) ≈ 1.37 (Pr) to 0.89 (Nd) and 0.72 (Sm). Temperature dependence of the interatomic distances in Ln_2CuO_4 shows significantly lower expansion rate of the chemical bond between Pr and oxygen atoms (O1) belonging to CuO_2-planes (TEC(Pr–O1)= 11.7 ppm K^{-1}) in comparison with other cuprates: TEC (Nd–O1)=15.2 ppm K^{-1} and TEC (Sm–O1)= 15.1 ppm K^{-1}. High-temperature electrical conductivity of Pr_2CuO_4 is the highest one in the whole studied temperature range (298–1173 K): 0.1–108 S/cm for Pr_2CuO_4, 0.07–23 S/cm for Nd_2CuO_4 and 2×10^{-4}–9 S/cm for Sm_2CuO_4. The trace diffusion coefficient (D_T) of oxygen for Pr_2CuO_4 determined by isotopic exchange depth profile (IEDP) technique using secondary ion mass spectrometry (SIMS) varies in the range 7.2×10^{-13} cm^2/s (973 K) and 3.8×10^{-10} cm^2/s (1173 K) which are in between those observed for the manganese and cobalt-based perovskites.

1. Introduction

Nowadays solid oxide fuel cells (SOFCs) are considered as one of the alternative to traditional hydrocarbons sources of energy due to their high efficiency and excellent fuel flexibility [1,2]. They are operating at high temperature up to 1273 K and this creates numerous problems such as chemical stability, matching of the thermal expansion coefficients (TEC) between the components of the SOFC, etc. [3–5]. Therefore, efforts are directed to the creation of the so-called intermediate temperature SOFC (IT-SOFC) with operation temperatures down to 773 K [6]. However, at such low temperature efficiency of the traditional electrode materials ((La,Sr)MnO_3 (LSM) for cathode and Ni–(Zr,Y)O_{2-x} (YSZ) for anode) dramatically decreases and novel electrode materials with improved properties are needed.

A number of efforts were made to prepare oxide compounds having superior characteristics in comparison with the widely used LSM cathode material. Recently, layered cuprates have attracted attention for the application in high-temperature electrochemical devices. Some of them show high total conductivity up to ~800 S/cm at 1073 K as, for example, $La_{0.7}Sr_{0.3}CuO_{2.5-y}$ [7]. Main drawbacks of the cuprates as cathode materials in SOFC are high TEC up to 17.9 ppm K^{-1} for $La_{1-x}Sr_xCuO_{2.5-y}$ [8] or 16.0 ppm K^{-1} for $La_2SrCu_2O_{6+y}$ [9] and high chemical activity toward reaction with electrolyte [8]. One of the reasons for such behavior could be instability at high temperature of oxides with copper in high oxidation state > +2. Therefore, it is expectable that cuprates with Cu^{2+} only could have better properties for high-temperature applications. Indeed, La_2CuO_4 has average TEC as low as 12.3 ppm K^{-1}, however, exhibits quite low conductivity at high temperature (~15 S/cm at 1200 K) [10].

Depending on the ionic radius of the rare-earth cation, Ln_2CuO_4 cuprates are known to crystallize in different structure types. La_2CuO_4 with large La^{3+} cation (Fig. 1A) crystallizes in the K_2NiF_4-type structure (so called T-phase), while other cuprates with smaller Ln^{3+} cations, have Nd_2CuO_4-type structure (T′-phase) (Fig. 1B). Although the high-temperature properties of the La_2CuO_4 are well studied, much less information is available for other Ln_2CuO_4 cuprates. However, one can expect that these compounds could be

* Corresponding author. Fax: +7 495 9394788.
E-mail addresses: istomin@icr.chem.msu.ru, istomin@inorg348-1.chem.msu.ru (S.Ya. Istomin).

0022-4596/$ - see front matter © 2011 Elsevier Inc. All rights reserved.
doi:10.1016/j.jssc.2011.01.035

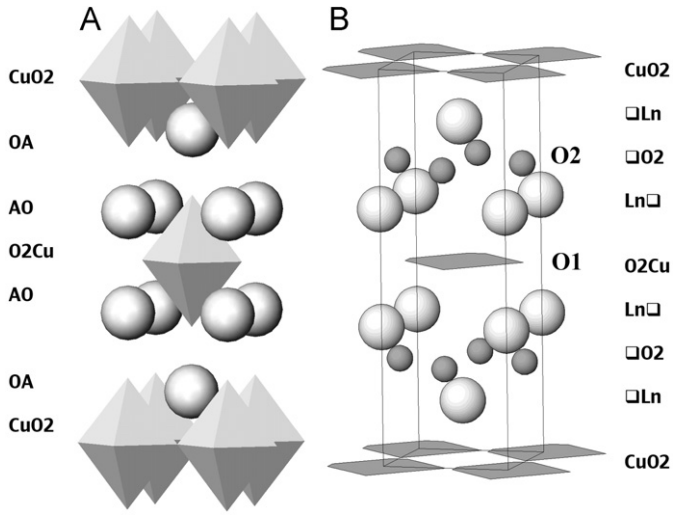

Fig. 1. The crystal structures of T-(K_2NiF_4) (A) and T′-phases (B).

of interest since Ce-doped $Nd_2CuO_{4\pm\delta}$ with T′-structure was found to exhibit promising properties for SOFC cathode application [11].

In the present paper, we report on the study of the thermal expansion, high-temperature electrical conductivity and high-temperature crystal structure of the cuprates Ln_2CuO_4, *Ln*=Pr, Nd and Sm performed in order to evaluate their possible use as cathode materials in SOFC. For Pr_2CuO_4 we have also determined oxygen trace diffusion and surface exchange coefficients using the diffusion of the isotope ^{18}O detected by secondary ion mass spectrometry (SIMS).

2. Experimental

Ln_2CuO_4, *Ln*=Pr, Nd and Sm were synthesized by annealing of the stoichiometric mixtures of $Nd(Sm)_2O_3$ or Pr_6O_{11} and CuO in air at 1273 K, 20 h (*Ln*=Pr, Nd) and 1323 K, 50 h (Sm). Copper oxide was prepared by decomposition of $(CuOH)_2CO_3$ at 573 K. Oxygen content of the cuprates was determined by iodometric titration.

Phase purity of the compounds was checked by X-ray powder diffraction (XRD) recorded in Huber G670 Guinier diffractometer (Cu$K\alpha_1$ radiation, image foil detector). High-temperature X-ray powder diffraction (HT XRD) data were collected in air using Bruker D8-Advance diffractometer (Cu$K\alpha_1$ radiation, Vantec PSD) in reflection mode equipped with high-temperature camera XRK-900 (Anton Paar). Crystal structures of the cuprates at different temperatures were refined by Rietveld method using TOPAS-3 program package.

Netzsch 402C dilatometer operated in air (298–1173 K, 10 K/min) was used for the thermal expansion coefficient measurements. For the thermal expansion measurements oxide powders were pressed into pellets 8 mm in diameter and 5–5.5 mm in height and annealed at 1343 K.

High-temperature electrical conductivity of the ceramic samples was measured in air by a standard 4-probe method in the temperature range of 298–1173 K. The samples have a typical shape of a disk with ~20 mm diameter and 1–2 mm thickness. The contacts were made from platinum wire (d~0.2 mm) placed in alumina tube and were pressed independently to the surface of the sample by separate individual springs situated at the top of the quartz sample holder kept at room temperature. The contacts were arranged in a line with 5–6 mm spacing between them. The influence of undesirable thermoelectric power was omitted by subtracting two successive voltage values on the potential contacts (the inner pair) measured at opposite current directions. The resulting resistivity value was recalculated into specific resistance using the approach developed in [12].

Dense ceramic samples for SIMS study were prepared by spark plasma sintering (SPS). 2–2.4 g of Pr_2CuO_4 powders were filled into a graphite die with an inner diameter of 12 mm. The temperature was measured with an optical pyrometer focused on the surface of the graphite die and automatically regulated from 873 to 1273 K or 1323 K at a heating rate of 50 K/min. The temperature of 873 K was reached via a preset heating program by 4 min. The holding time was set to 5 min at the final temperature. A constant uniaxial pressure of 50 MPa was applied during the whole sintering period. After sintering, a surface layer (about 0.5 mm) of the ceramic sample was removed by polishing with sandpaper and ultrasonically cleaned in acetone to remove polish residues. Phase purity of the ceramic sample was checked by XRD.

The ^{18}O penetration profiles were determined on a TOF-SIMS 5 instrument operated in depth profile mode, with a 45° incidence 25 keV Bi^+ primary ion beam; the crater depth was measured after the SIMS analysis by surface profilometry (Taylor–Hobson Talystep).

3. Results and discussion

3.1. Thermal expansion properties and high-temperature crystal structure of Ln_2CuO_4, Ln=Pr, Nd and Sm

XRD patterns of Ln_2CuO_4, *Ln*=Pr, Nd and Sm at room temperature were fully indexed in tetragonal I-centered unit cells with parameters a=3.9609(1) Å; c=12.2210(6) Å (*Ln*=Pr); a=3.9414(1) Å; c=12.1626(1) Å (*Ln*=Nd) and a=3.9136(2) Å; c=11.9708(5) Å (*Ln*=Sm), which correspond to the literature data for these phases [13]. A clear decrease of the unit cell dimensions is observed with decreasing of the ionic radius of the rare-earth cation from Pr^{3+} to Sm^{3+} (r^{3+}_{Pr}=1.14 Å, r^{3+}_{Nd}=1.12 Å, r^{3+}_{Sm}=1.09 Å, CN=8 [14]). Oxygen content of the phases, as determined by iodometric titration, corresponds within e.s.d. to the stoichiometric composition.

Thermal expansion curves for Ln_2CuO_4, *Ln*=Pr, Nd and Sm ceramic samples obtained by dilatometry are shown in Fig. 2. Calculated linear thermal expansion coefficients (TEC) are given in Table 1. Temperature dependences of the unit cell parameters

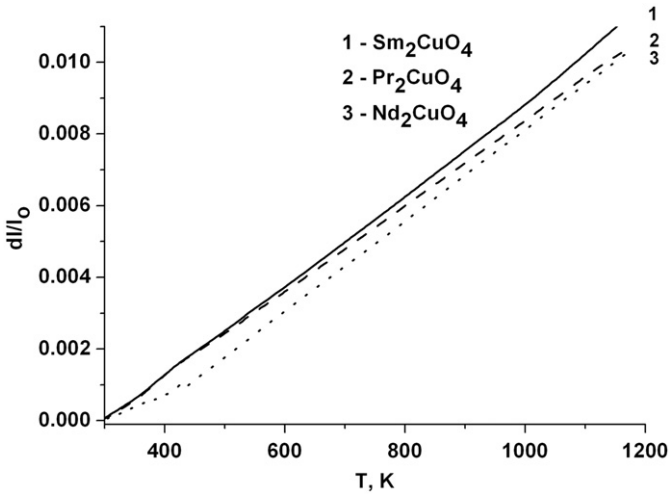

Fig. 2. Thermal expansion curves for Ln_2CuO_4, *Ln*=Pr, Nd and Sm.

Table 1
Thermal expansion coefficients (TEC) (in ppm K^{-1}) of Ln_2CuO_4, Ln=Pr, Nd and Sm calculated from dilatometry data (TEC(dil)) and from HT XRD (TEC($V^{1/3}$)) together with TEC of the individual unit cell parameters and Ln–O interatomic distances.

	Pr_2CuO_4	Nd_2CuO_4	Sm_2CuO_4
TEC(dil)	11.8	12.6	12.6
TEC($V^{1/3}$)	11.9	13.0	12.9
TEC(a)	13.0	12.5	11.5
TEC(c)	9.5	14.0	15.9
TEC(Ln–O1)	11.7	15.2	15.1
TEC(Ln–O2)	11.9	10.7	11.1

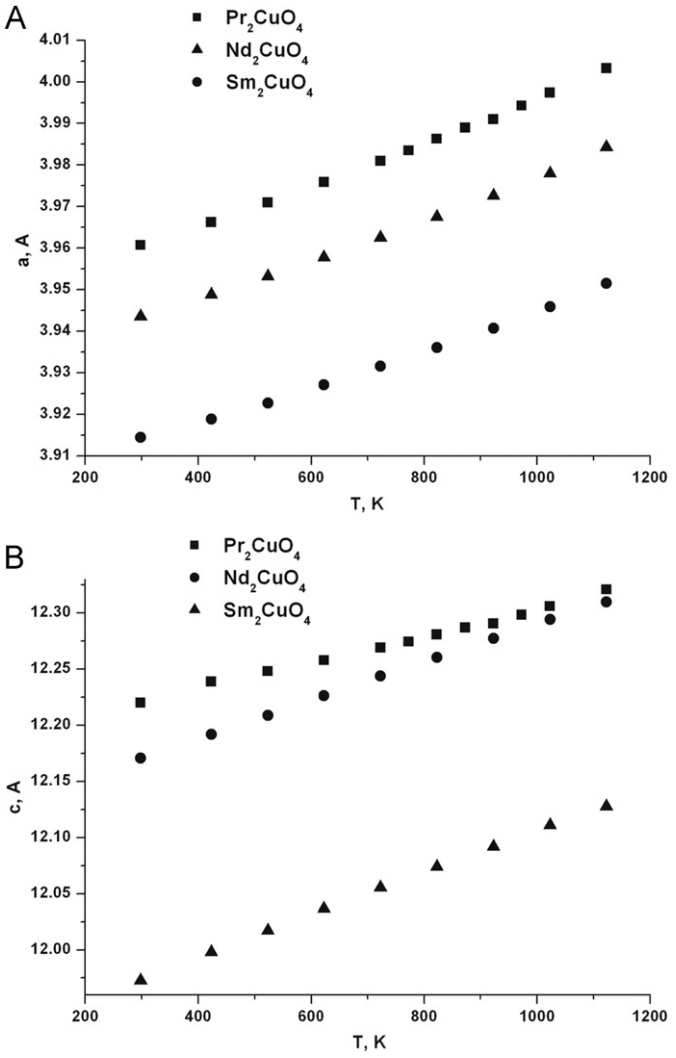

Fig. 3. Temperature dependence of the unit cell parameters of Ln_2CuO_4, Ln=Pr, Nd and Sm.

of Ln_2CuO_4, Ln=Pr, Nd and Sm, as determined from high-temperature XRD data, are shown in Figs. 3A and B. TEC values of the cuprates calculated from the temperature dependence of unit cell volume ($V^{1/3}$) correspond well to those from the dilatometry data (Table 1). It should be mentioned that they are higher in the comparison with those determined using dilatometry in the same temperature range by Kharton et al. [15] for Pr_2CuO_4 (10.21(7) ppm K^{-1}) and Nd_2CuO_4 (10.1(2) ppm K^{-1}).

Calculated TEC values along a-axis (TEC(a)) and c-axis (TEC(c)) of Ln_2CuO_4 are given in Table 1. Decreasing of TEC(a) from Pr to Sm is correlated with decreasing copper–oxygen in-plane bond length as can be observed from the unit cell dimensions of Ln_2CuO_4 given above. At the same time, TEC(c) increases from Pr_2CuO_4 to Sm_2CuO_4. Moreover, for Pr_2CuO_4 TEC(a) is substantially higher in comparison with TEC(c): TEC(a)/TEC(c) ≈ 1.37 (Table 1). Opposite situation is observed for Nd_2CuO_4 and Sm_2CuO_4 where TEC(a)/TEC(c) ≈ 0.89 (Nd) and 0.72 (Sm).

In order to reveal structural reason for such behavior, high temperature crystal structures of Ln_2CuO_4 were refined. Initial atomic coordinates were taken from the room-temperature data for Pr_2CuO_4 (S.G. $I4/mmm$) [16]. As an example, results of the Rietveld refinement's for Ln_2CuO_4, Ln=Pr, Nd and Sm using XRD data recorded at 298 and 1123 K are given in Table 2. Observed, calculated and difference XRD profiles for Ln_2CuO_4 at the selected temperatures are given in Fig. 4.

The sequence of layers in T′-structure can be represented as $\cdots CuO_2-\square Ln-\square O_2-Ln\square-O_2Cu-\cdots$ (Fig. 1B). There are two crystallographically distinct oxygen atoms in the T′-structure belonging to CuO_2 (oxygen O1) layers and to Ln_2O_2 block (oxygen O2). Both oxygen atoms occupy special positions in S.G. $I4/mmm$ and the only refinable atomic parameter is z-coordinate of Ln^{3+} cation. Temperature dependences of the Ln–O1 and Ln–O2 interatomic distances are shown in Fig. 5, corresponding values of the temperature expansion rates are given in Table 1. One can observe that temperature induced expansion rate of Pr–O1 bond length is considerably smaller in comparison with the Nd–O1 and Sm–O1 ones. Moreover, at $T > 873$ K the difference between the Pr–O1 and Nd–O1 distances practically disappears. TEC of the long Pr–O1 bond (~2.68 Å at 298 K) is comparable with that for the shorter Pr–O2 one (~2.34 Å at 298 K), while for both Sm_2CuO_4 and Nd_2CuO_4 TEC of Ln–O1 bond is about 40% higher in comparison with Ln–O2 one (Table 1). It indicates to the presence of the stronger, in comparison with other rare-earth cations, interactions between praseodymium and oxygen atoms from the CuO_2 layer. Such conclusion could have been supported by band structure calculations but to our knowledge no data are available for Pr_2CuO_4. However, detailed band structure calculations were performed for the layered cuprate $PrBa_2Cu_3O_7$ [17,18]. In the band structure of $PrBa_2Cu_3O_7$, in comparison with analogs with other rare-earth cations, there is a strong hybridization near the Fermi level of the 4f states of Pr and 2p states of O. Due to similar arrangement of the Pr cations and neighboring CuO_2 planes in both 123- and T′-phases, one may propose the presence of alike features in the electronic structure of Pr_2CuO_4. Therefore, we can speculate that such electronic structure feature may be a reason for anomalous high-temperature behavior of Pr_2CuO_4 in comparison with other rare-earth cuprates.

3.2. High-temperature electrical conductivity of Ln_2CuO_4

High-temperature electrical conductivity behavior of the Ln_2CuO_4 ceramic samples was studied in air in the temperature range of 298–1173 K by four-probe method. Conductivity of all samples increases with temperature thus indicating a semiconductor-like behavior (Fig. 6). Conductivity of Pr_2CuO_4 is the highest one among studied cuprates in the whole temperature range: 0.1–108 S/cm for Pr_2CuO_4, 0.07–23 S/cm for Nd_2CuO_4 and 2×10^{-4}–9 S/cm for Sm_2CuO_4. In contrast, at 298–1273 K La_2CuO_4 with T-structure exhibits temperature-independent type of conductivity with $\sigma \sim 15$ S/cm [10,19].

Two temperature ranges (298–773 and 773–1173 K) with activation-like behavior can be observed for all $\sigma(T)$ dependences (Fig. 6). Their existence can be explained by the change from p- to n-type conductivity with increasing temperature as observed by Scavini et al. [20] in the high-temperature study of Nd_2CuO_4.

Table 2
Results of the Rietveld refinement's for Ln_2CuO_4, Ln=Pr, Nd and Sm using XRD data recorded at 298 and 1123 K.

Compound	T (K)	Unit cell parameters (Å)	R_{wp}, R_p, χ^2	Atomic coordinates, B_{iso} (Å^2)[a]
Pr_2CuO_4	298	a=3.96072(3), c=12.2200(1)	0.0679, 0.0535, 1.05	z(Pr)=0.35187(8), B_{iso}(Pr)=0.26(6); B_{iso}(Cu)=0.59(8)
	1123	a=4.00323(3), c=12.3208(1)	0.0665, 0.0527, 1.08	z(Pr)=0.35174(9), B_{iso}(Pr)=1.23(8); B_{iso}(Cu)=1.63(1)
Nd_2CuO_4	298	a=3.94357(3), c=12.1708(1)	0.0655, 0.0519, 1.04	z(Nd)=0.35118(9), B_{iso}(Nd)=0.34(7); B_{iso}(Cu)=0.3(1)
	1123	a=3.98425(4), c=12.3096(2)	0.0623, 0.0494, 1.04	z(Nd)=0.3510(1), B_{iso}(Nd)=1.2(1); B_{iso}(Cu)=1.0(2)
Sm_2CuO_4	298	a=3.91445(6), c=11.9727(3)	0.0517, 0.0412, 1.03	z(Sm)=0.3508(1), B_{iso}(Sm)=0.7(1); B_{iso}(Cu)=0.5(1)
	1123	a=3.95151(5), c=12.1278(2)	0.0481, 0.0382, 1.04	z(Sm)=0.3503(2), B_{iso}(Sm)=1.4(1); B_{iso}(Cu)=1.2(2)

[a] Ln and Cu are at 4e position (0, 0, z) and 2a (0, 0, 0) positions, respectively; oxygen atoms O1 and O2 are at special positions 4c (0, 1/2, 0) and 4d (0, 1/2, 1/4), respectively. Atomic displacement parameters for O1 and O2 were fixed at B_{iso}=1 Å^2 and were not refined.

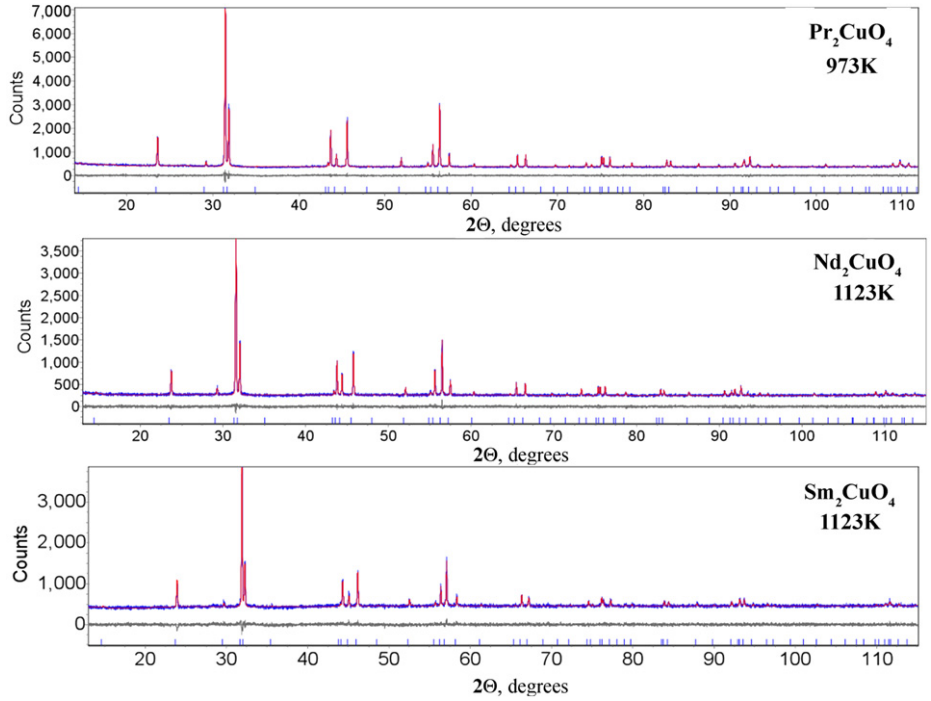

Fig. 4. Observed, calculated and difference between them XRD profiles for Ln_2CuO_4, Ln=Pr (T=973 K), Nd (T=1123 K) and Sm (T=1123 K).

In both ranges temperature dependencies of conductivity are perfectly fitted by Arrhenius law with activation energies (E_A) listed in Table 3. The conductivity of Pr_2CuO_4 rapidly increases with temperature in low temperature range and shows a saturation behavior at high temperature. Increasing of the transition temperature between ranges from Pr to Sm is likely to correlate with the value of charge-transfer gap, which increases from Pr_2CuO_4 to Sm_2CuO_4 [21]. Substantial increase of the activation energy is observed for Nd_2CuO_4 and Sm_2CuO_4 in high-temperature range in comparison with low-temperature one. For Pr_2CuO_4 the situation is opposite where E_A decreases nearly by ~50% in comparison with low temperature range. These results are in good agreement with the data by Goodenough [22] and George et al. [19]. The reason for anomalous high-temperature conductivity behavior of Pr_2CuO_4 could also be connected with the specific feature of the electronic structure mentioned above.

3.3. Oxygen diffusion and surface exchange coefficients of Pr_2CuO_4

The oxygen diffusion coefficient D_T and the surface exchange coefficient k for Pr_2CuO_4 were determined by the isotopic exchange depth profile (IEDP) technique using SIMS after isotopic exchange of ^{18}O for ^{16}O in the ceramic samples.

Dense ceramic samples of Pr_2CuO_4 for SIMS study were prepared by SPS technique. Since the graphite was used as a pressure transmitting media in SPS experiment, color of the surface of the pellet after the sintering was non-uniform indicating the partial reduction of cuprate. XRD study of the pellet with the surface cleaned by sandpaper, showed an absence of the admixture phases. Density of the ceramic samples of Pr_2CuO_4, as determined by pycnometry, was 99.9% relative to X-ray density for the sample sintered at 1273 K and 99.6% for the sample sintered at 1323 K. Prior to ^{18}O exchange annealing, samples were held at 973, 1073, 1123 and 1173 K in air of normal isotopic abundance for a period of time approximately one order of magnitude longer then the tracer annealing time. This was carried out to ensure that the material was in chemical equilibrium at the desired temperature and oxygen partial pressure (in this study all annealings were carried out at a nominal oxygen pressure of 0.2 atm). The air was then removed, and labeled oxygen (95% enriched $^{18}O_2$) introduced. Annealing time was 10–12 min for the samples studied at 1073, 1123 and 1173 and 9 h for 973 K.

As an example, the ^{18}O isotopic concentration depth profile of Pr_2CuO_4 annealed at 1073 K is given in Fig. 7. The oxygen tracer diffusion (D_T) and surface exchange (k) coefficients were determined by non-linear least squares regression based on fitting of the diffusion profiles using the Crank relation, solution of the

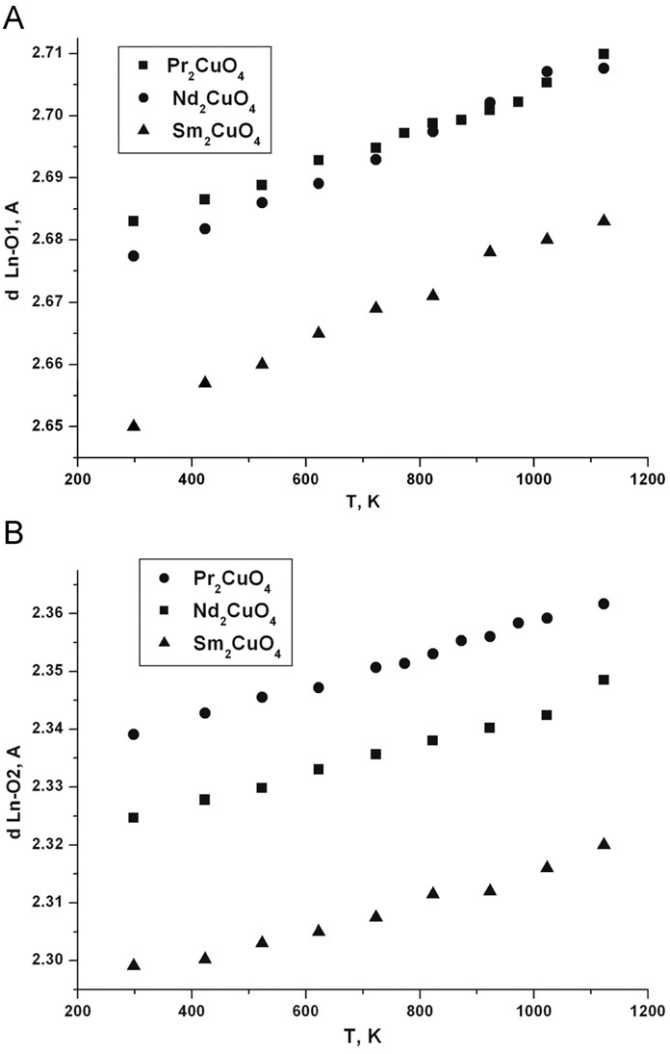

Fig. 5. Temperature dependence of the *Ln*–O1 and *Ln*–O2 interatomic distances in the crystal structures of Ln_2CuO_4, *Ln*=Pr, Nd and Sm.

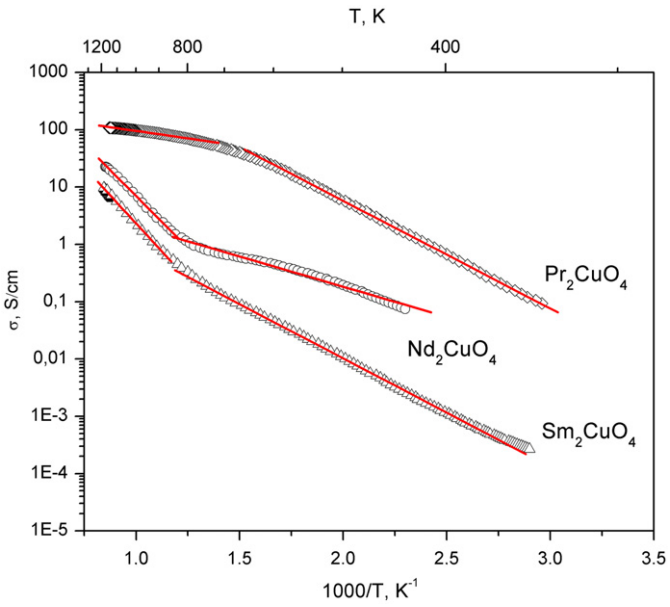

Fig. 6. Temperature dependence of the electrical conductivity (σ) for cuprates with T′-structure (1—Pr_2CuO_4, 2—Sm_2CuO_4, 3 – Nd_2CuO_4). Solid lines refer to the fit by the Arrhenius law ($\sigma(T)\sim\exp(-E_A/k_BT)$).

Table 3
Activation energies (E_A) for the high-temperature electrical conductivity of Ln_2CuO_4, *Ln*=Pr, Nd and Sm.

Compound	Temperature range (K)	Activation energy, E_A (eV)
Pr_2CuO_4	298–723	0.37 ± 0.02
	723–1173	0.18 ± 0.02
Nd_2CuO_4	298–873	0.26 ± 0.02
	873–1173	0.78 ± 0.02
Sm_2CuO_4	298–873	0.42 ± 0.02
	873–1173	0.83 ± 0.02

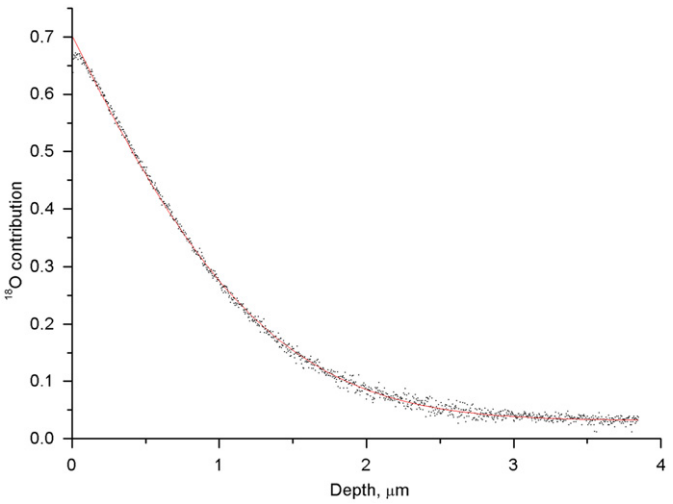

Fig. 7. O^{18} penetration profile determined for Pr_2CuO_4 at 1073 K. The points refer to experimental data, and the curve for the fitting results.

Table 4
Calculated values of D_T and k for Pr_2CuO_4 at various temperatures.

T (K)	D_T (cm²/s)	k (cm/s)
973	7.2×10^{-13}	1.2×10^{-8}
1073	1.1×10^{-11}	2.3×10^{-7}
1123	5.7×10^{-11}	2.6×10^{-7}
1173	3.8×10^{-10}	8.7×10^{-7}

Fick's second law of the diffusion, similar to the procedure described in Refs. [10,23]. Calculated values of D_T and k are given in Table 4. Dependences of bulk oxygen tracer diffusion and surface exchange coefficients on reverse temperature are given in Fig. 8. They can be perfectly fitted by Arrhenius law with activation energies (E_A) for oxygen tracer diffusion and for surface exchange coefficients 290 ± 28 and 197 ± 28 kJ mol^{-1}, respectively.

Calculated value of activation energy for oxygen trace diffusion in Pr_2CuO_4 is much closer to that for the perovskites with low oxide-ion mobility like lanthanum–strontium manganate (250–300 kJ mol^{-1}) in comparison with cobaltates (100–200 kJ mol^{-1}) [23,24]. At the same time, the observed values of D_T are by several orders of magnitude higher in comparison with the strontium doped manganite $La_{1-x}Sr_xMnO_3$ for which they are $\sim10^{-12}$–10^{-13} cm²/s at 1173 K and $\sim10^{-14}$–10^{-15} cm²/s at 1073 K [24,25]. However, values of D_T for Pr_2CuO_4 are much lower in comparison with good oxide-ion conductors like cobaltates (4×10^{-8} cm²/s (1173 K); 2×10^{-8} cm²/s (1073 K) for $La_{0.8}Sr_{0.2}CoO_3$ [24]) and Ln_2NiO_{4+y}, *Ln*=La, Pr and Nd$\sim10^{-8}$ cm²/s at 1073 K [26–28]. Moreover, observed values of the tracer diffusion coefficient for Pr_2CuO_4

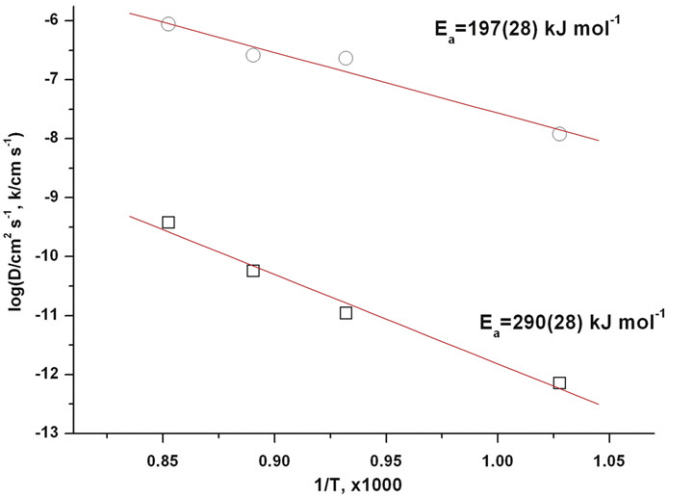

Fig. 8. Bulk oxygen tracer diffusion and surface exchange coefficients obtained for Pr_2CuO_4 ceramics as a function of inverse temperature. Circles refer to surface exchange, squares—to oxygen tracer diffusion coefficients.

are much lower in comparison with La_2CuO_4, for which a value of $\sim 10^{-8}$ cm^2/s was reported already at 973 K [10]. One can explain it by substantial difference in the crystal structures of T and T′-phases which influences on the mechanism and energetics of the oxygen diffusion in the compounds. In both crystal structures there are slabs formed by Ln^{3+} cations in which there are tetrahedral and octahedral voids for oxygen atoms. In the crystal structure of T-phase octahedral voids are fully occupied by oxygen atoms while tetrahedral sites are empty or partially occupied like in the case of La_2NiO_{4+y} (see, for example, [29]). Opposite situation is observed for the T′-phase where tetrahedral sites are fully occupied by oxygen while octahedral sites remain empty. This leads to the different coordination of copper in T- and T′-phases: octahedron for T- and square for T′ (see Fig. 1A and B). In the T-structure the distances between transition metal cation and axial oxygen anion are much longer in comparison with the equatorial ones. For example, in La_2CuO_4 $d_{Cu-O(eq)}\sim 1.90$ Å, $d_{Cu-O(ax)}\sim 2.43$ Å [30] and in La_2NiO_4 $d_{Ni-O(eq)}\sim 1.95$ Å, $d_{Ni-O(ax)}\sim 2.26$ Å [31]. This weakens interactions between transition metal and axial oxygen atoms and makes easier migration of oxygen in the structure. Recently, it was established that migration of oxygen between octahedral and tetrahedral sites in La_2O_2 block plays a major role in the mechanism of oxygen diffusion in La_2NiO_{4+y} [32,33]. In the crystal structure of T′-phase the distance between copper and empty octahedral site in the Ln_2O_2 block is substantially shorter (for example, in Pr_2CuO_4 it is equal to 1.81 Å which is much smaller in comparison with typical Cu^{2+}–O bond length). This should hamper oxygen diffusion in T′-phases by the migration of oxygen between octahedral and tetrahedral sites in the Ln_2O_2 block. The lower diffusibility of oxygen in T′-phases in comparison with T-phases is supported by the substantially lower oxygen permeation fluxes observed through ceramic membranes of Nd_2CuO_4 and Pr_2CuO_4 in comparison with La_2CuO_4 [15].

Unfortunately, it is hard to compare the observed data for Pr_2CuO_4 with other T′-phase since, to our knowledge, no data for the oxygen tracer diffusion determined by SIMS is available for them. However, some years ago Idemoto et al. [34,35] reported on the study of the oxygen chemical diffusion on both poly- and single crystal samples of Nd_2CuO_4 by means of thermomicrobalance. They have reported high values of the oxygen chemical diffusion coefficient $\sim 10^{-5}$–10^{-6} cm^2/s at 923–1173 K and calculated values of self-diffusion coefficient are $\sim 10^{-8}$ cm^2/s at 1073–1173 K. However, due to the high dependence of the chemical diffusion coefficient on the microstructure of the sample, these values could be overestimated and it would be valuable to obtain values of the oxygen tracer diffusion for Nd_2CuO_4 by SIMS.

4. Conclusions

Our work showed that the high-temperature properties of the cuprates with T′-type structure (Ln_2CuO_4, Ln=Pr, Nd, Sm) depend strongly on the type of the rare-earth cation. Study of the thermal expansion behavior of the layered cuprates Ln_2CuO_4, Ln=Pr, Nd and Sm with T′-structure revealed its anisotropy along the a- and c-axis of the tetragonal structure. However, this anisotropy is different for Ln=Nd, Sm with TEC(a) < TEC(c) and for Pr_2CuO_4 with TEC(a) > TEC(c). High-temperature XRD study of the crystal structures of these layered cuprates, leads to the conclusion that anomalous behavior of Pr_2CuO_4 in comparison with Nd and Sm-based cuprates is due to the stronger bonding between Pr^{3+} cations and oxygen atoms from the CuO_2 planes. High-temperature electrical conductivity of the studied cuprates increases with the rare-earth cation size from Sm to Pr. Measurements of the oxygen trace diffusion coefficient for Pr_2CuO_4 by IEDP SIMS revealed values between those reported for the LSM and cobalt-based perovskites (La,Sr)CoO_{3-y}. From the viewpoint of the application as cathode in IT-SOFC, rare-earth cuprates Ln_2CuO_4, Ln=Pr, Nd and Sm have advantages over other layered cuprates due lower TEC ($\sim$12–13 ppm K^{-1}). However, conductivity of Ln_2CuO_4, Ln=Pr, Nd and Sm at T < 973 K is high enough (> 10 S/cm) for Pr_2CuO_4 only. At the same time the "compressed" Pr_2O_2 slab in the Pr_2CuO_4 crystal structure with small separation between available empty octahedral sites and Pr cations hamper oxygen anion diffusion and results in small value of the oxygen trace diffusion coefficient in this phase compared to those values obtained for the T-phases (La_2CuO_4 and Nd_2NiO_{4+y}) where this separation is significantly larger. This property seems to be one of the main drawbacks of the cuprates with T′-type structure and should limit their use as cathode in IT-SOFC. The possible way to overcome this problem can be cation replacements in both sites of the structure, which can extend the Pr_2O_2 slab resulting in higher oxygen mobility.

Acknowledgments

This work was partially supported by RFBR (#08-03-00919) and by the Swedish Research Council and Swedish Institute (Visbyprogramme).

References

[1] B.C.H. Steele, A. Heinzel, Nature 414 (2001) 345–352.
[2] S.M. Haile, Acta Mater. 51 (2003) 5981–6000.
[3] H. Tu, U. Stimming, J. Power Sources 127 (2004) 284–293.
[4] S.P.S. Badwal, Solid State Ionics 143 (2001) 39–46.
[5] N.Q. Minh, J. Am. Ceram. Soc. 76 (1993) 563–588.
[6] J.M. Ralph, A.C. Schoeler, M. Krumpelt, J. Mater. Sci. 36 (2001) 1161–1172.
[7] H.-C. Yu, K.-Z. Fung, Mater. Res. Bull. 38 (2003) 231–239.
[8] H.-C. Yu, K.-Z. Fung, J. Power Sources 133 (2004) 162–168.
[9] G.N. Mazo, M.S. Kaluzhskikh, S.N. Savvin, L.S. Leonova, N.V. Lyskov, Yu.A. Dobrovol'skii, Russ. J. Electrochem. 45 (2009) 450–455.
[10] E. Boehm, J.-M. Bassat, M.C. Steil, P. Dordor, F. Mauvy, J.-C. Grenier, Solid State Sci. 5 (2003) 973–981.
[11] M. Soorie, S.J. Skinner, Solid State Ionics 177 (2006) 2081–2086.
[12] H.R. Kokabi, J. Provost, G. Desgardin, Rev. Sci. Instrum. 64 (1993) 1549–1553.
[13] J.F. Bringley, S.S. Trail, B.A. Scott, J. Solid State Chem. 86 (1990) 310–322.
[14] R.D. Shannon, Acta Crystallogr. A 32 (1976) 751.
[15] V.V. Kharton, A.P. Viskup, A.V. Kovalevsky, E.N. Naumovich, F.M.B. Marques., Solid State Ionics 143 (2001) 337–353.
[16] D.E. Cox, A.I. Goldman, M.A. Subramanian, J. Gopalakrishnan, A.W. Sleight, Phys. Rev. B 40 (1989) 6810–6998.

[17] R. Fehrenbacher, T.M. Rice, Phys. Rev. Lett. 70 (1993) 3471–3474.
[18] A. Tavana, M. Shirazi, M. Akhavan, Phys. Status Solidi B 246 (2009) 2287–2293.
[19] A.M. George, I.K. Gopalakrishnan, M.D. Karkhanavala, Mater. Res. Bull. 9 (1974) 721–725.
[20] M. Scavini, G. Chiodelli, G. Spinolo, G. Flor, Physica C 230 (1994) 412–418.
[21] A. Tsukada, H. Shibata, M. Noda, H. Yamamoto, M. Naito, Physica C 445–448 (2006) 94–96.
[22] J.B. Goodenough, Mater. Res. Bull. 8 (1973) 423–432.
[23] A. Kilner, R.A. De Souza, I.C. Fullarton, Solid State Ionics 86–88 (1996) 703–709.
[24] S. Carter, A. Selcuk, R.J. Chater, J. Kajda, J.A. Kilner, B.C.H. Steele, Solid State Ionics 53–56 (1992) 597–605.
[25] R.A. De Souza, J.A. Kilner, J.F. Walker, Mater. Lett. 43 (2000) 43–52.
[26] C.N. Munnings, S.J. Skinner, G. Amow, P.S. Whitfield, I.J. Davidson, Solid State Ionics 176 (2005) 1895–1901.
[27] J.M. Bassat, P. Odier, A. Villesuzanne, C. Marin, M. Pouchard, Solid State Ionics 167 (2004) 341–347.
[28] E. Boehm, J.-M. Bassat, P. Dordor, F. Mauvy, J.-C. Grenier, Ph. Stevens, Solid State Ionics 176 (2005) 2717–2725.
[29] J.B. Goodenough, A. Manthiram, J. Solid State Chem. 88 (1990) 115–139.
[30] P.G. Radaelli, D.G. Hinks, A.W. Mitchell, B.A. Hunter, J.L. Wagner, B. Dabrowski, K.G. Vandervoort, H.K. Viswanathan, J.D. Jorgensen, Phys. Rev. B 49 (6) (1994) 4163–4175.
[31] J.D. Jorgensen, B. Dabrowski, S. Pei, D.R. Richards, D.G. Hinks, Phys. Rev. B 40 (1989) 2187–2199.
[32] A. Chroneos, D. Parfitt, J.A. Kilner, R.W. Grimes, J. Mater. Chem. 20 (2010) 266–270.
[33] R. Sayers, R.A. De Souza, J.A. Kilner, S.J. Skinner, Solid State Ionics 181 (2010) 386–391.
[34] Y. Idemoto, K. Fueki, M. Sugiyama, J. Solid State Chem. 92 (1991) 489–495.
[35] Y. Idemoto, K. Uchida, K. Fueki, Physica C 222 (1994) 333–340.